ORIGINAL PAPER

A force field for dynamic Cu-BTC metal-organic framework

Lei Zhao · Qingyuan Yang · Qintian Ma ·
Chongli Zhong · Jianguo Mi · Dahuan Liu

Abstract A new force field that can describe the flexibility of Cu-BTC metal-organic framework (MOF) was developed in this work. Part of the parameters were obtained using density functional theory calculations, and the others were taken from other force fields. The new force field could reproduce well the experimental crystal structure, negative thermal expansion, vibrational properties as well as adsorption behavior in Cu-BTC. In addition, the bulk modulus of Cu-BTC was predicted using the new force field. We believe the new force field is useful in understanding the structure-property relationships for MOFs, and the approach can be extended to other MOFs.

Keywords Cu-BTC · Flexibility · Force field · Metal-organic framework · Molecular simulation

Introduction

Metal-organic frameworks (MOFs) have been recognized as a new family of nanoporous materials with a wide range of possible applications in gas storage, sensing, separation and catalysis, etc. [1–3]. Molecular modeling is a powerful tool to predict properties (such as molecular diffusion and adsorption) and provide insights into the molecular level details of the underlying mechanisms, which could guide the future rational design and synthesis of tailored MOF materials.

Extensive molecular simulations have been performed on the adsorption and diffusion of gases in MOFs [4–10]. However, most of them use rigid frameworks with the framework atoms in MOFs fixed in their experimentally determined crystallographic positions, and the standard force fields such as UFF [11], Dreiding [12], OPLS [13], and CVFF [14] were used. Since MOFs are flexible and may exhibit substantial changes in unit cell volume upon external stimulus such as temperature and guest molecules [15–17], force fields that can describe the dynamic behavior of MOFs are highly needed.

Up to date, several flexible force fields have been proposed for MOFs. Greathouse and Allendorf suggested a nonbonded force field for MOF-5 (also known as IRMOF-1). The mechanism of MOF-5 collapses upon water adsorption was studied [18], and the force field also correctly predicted a wide range of structural properties of this MOF, such as the negative thermal expansion property (NTE), elastic moduli and vibrational power spectra [19]. A similar strategy has been adopted by Dubbeldam et al., and NTE behavior of MOF-5 was reproduced very well using their extended force field [20]. Based on density functional theory (DFT) calculations and experimental data, Huang et al. developed a force field for MOF-5, and calculated the phonon thermal conductivity and vibrational power spectra [21]. Tafipolsky et al., on the other hand, parameterized the MM3 force field for MOF-5 based on DFT calculations [22]. The fully bonded model not only predicts the MOF-5 structure in agreement with the experimental value, but also reproduces quite well the self-diffusivity of benzene in MOF-5 as compared with rigid framework [23]. More recently, a new bonded force field was developed by Salles et al., which can describe the evolution of the unit cell volume of MIL-53(Cr) in good agreement with the experimental data [24].

L. Zhao · Q. Yang · Q. Ma · C. Zhong (✉) · J. Mi · D. Liu
Laboratory of Computational Chemistry, Department of Chemical Engineering, Beijing University of Chemical Technology,
Beijing 100029, China
e-mail: zhongcl@mail.buct.edu.cn

To date, most flexible force fields were developed for MOF-5, and there is no such force field available for Cu-BTC ($Cu_3(BTC)_2$ with BTC=benzene-1,3,5-tricarboxylate), one of the two most well-studied MOFs other than MOF-5. Cu-BTC was first reported by Chui et al. (Fig. 1a) [25], and has been widely studied for gas adsorption and diffusion [8, 26, 27]; it has a pocket/channel structure, which is more complex than MOF-5. Up to now, all the simulations were performed for rigid Cu-BTC frameworks using standard force fields. So, a new force field that can describe the flexibility of Cu-BTC was first developed in this work. In our force field, angle bending parameters around Cu were obtained using DFT calculations, with the other parameters taken from other force fields and some of them were adjusted slightly if necessary. The new force field was used

to calculate the crystal structure, NTE, vibrational properties as well as adsorption behavior in Cu-BTC and compared with experimental results. In addition, the bulk modulus of Cu-BTC was predicted using the new force field.
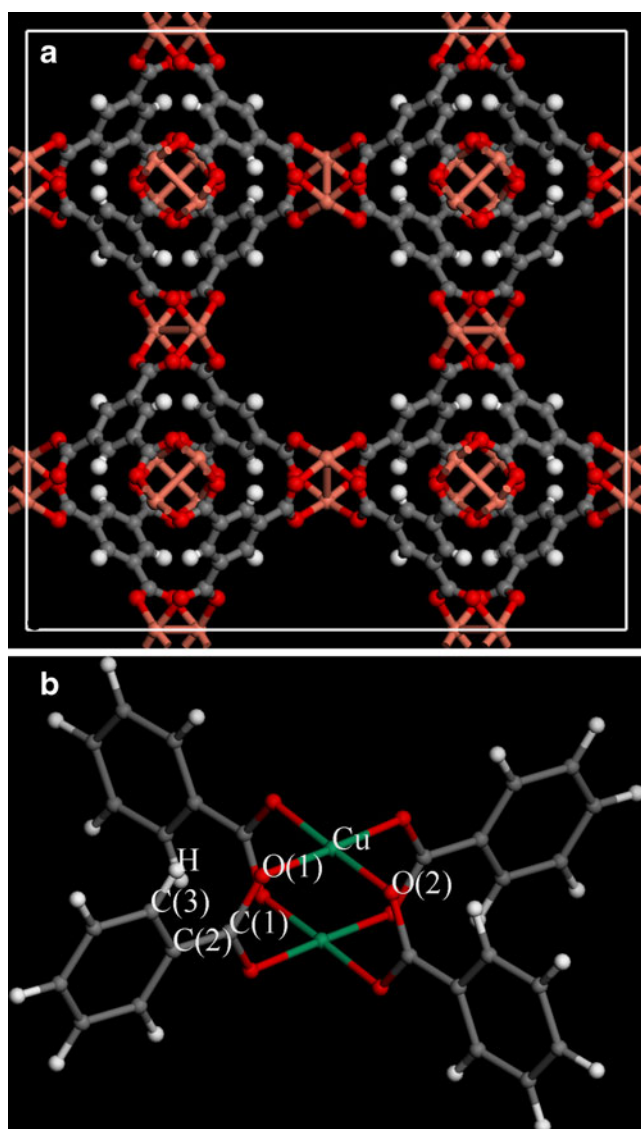
Computational details

DFT calculation

DFT calculations were employed to parameterize angle bending parameters around Cu. The model cluster of Cu-BTC used for DFT calculations is shown in Fig. 1b. It was fully optimized by DFT calculations using the unrestricted B3LYP functional. To determine the appropriate basis set, apart from two uniform basis sets 6-311G(d,p) and 6-311+G(d,p), two tailor-made basis sets were also adopted: the basis set LANL2DZ was used for atoms Cu, together with the 6–31G(d, p) basis set (Mixed I) or 6–311G(d,p) basis set (Mixed II) for the C, O and H atoms and the multiplicity is 3. The optimized structures were compared with experimental data, as shown in Table 1. It may be concluded that the basis set 6–311G(d,p) is the most suitable one that gives the smallest sum of squares error. Therefore, this basis set was adopted in our DFT calculations. In order to accurately calculate low vibrational modes, we used a more tight convergence criterion and a finer grid for the integration. All the quantum-mechanic calculations have been preformed with the Gaussian03 program suite [28].

MD simulation

To develop and check the force field for the dynamic Cu-BTC framework, molecular dynamics (MD) simulations in the *NPT* ensemble were performed to calculate its crystal structural properties. During the simulations, we maintained the pressure at 0.1 MPa and symmetry constraints were removed to make each lattice parameter vary independently. The Nose Hoover thermostat and barostat were used to maintain the temperature and pressure with the optimal

Fig. 1 (a) Unit cell structure of Cu-BTC; (b) The cluster for the DFT calculations and atom types

Table 1 Comparison of the predicted bond distances with experimental data [25]

Basis sets	Cu-O1	O-C1	C1-C2	C2-C3	s^2 (10^{-3})
6–311G(d,p)	1.950	1.270	1.491	1.399	0.25
6–311+G(d,p)	1.973	1.27	1.495	1.399	0.34
Mixed I	1.973	1.274	1.495	1.402	0.45
Mixed II	1.982	1.269	1.494	1.399	0.44
Experiment	1.952	1.252	1.500	1.397	

relaxation times 0.1 and 1.0 ps, respectively. Short-range and bonded energy terms were calculated every 0.5 fs, with a cutoff distance of 12 Å, and long-range electrostatic terms were calculated every 1 fs using an efficient particle-particle particle-mesh solver (pppm) [29]. The simulation system consisted of one unit cell of Cu-BTC containing 624 atoms and was equilibrated for 200 ps at 293 K followed by a 1000 ps for production. Test simulations using $2\times2\times2$ unit cells and longer time simulation (10 ns) gave equivalent results, but were deemed too expensive for the computational cost. Thermal expansion data were also obtained from a series of *NPT* simulations between 50 and 500 K, where the framework of Cu-BTC has been indicated to be stable by the experiment [25]. At each temperature, the system was equilibrated for 200 ps, and then sampled in another 1000 ps. The error bars of the lattice parameters were estimated by averaging the standard errors of 10 trajectories. Furthermore, to compare with the available experimental data for the vibrational frequencies, *NVE* simulation with the length of 40 ps was also performed on the equilibrated structure of Cu-BTC obtained above at 298 K. Atomic velocities were collected every 4 fs, a power spectrum was produced by a Fourier transform of the velocity autocorrelation function produces. The relation between energy and volume was obtained from a series of 1 ns *NVT* simulations at 300 K. In these simulations the isotropic lattice parameter was increased from 26.075 to 26.575 Å. All the MD simulations performed in this work were carried out using LAMMPS software package [30].

Hybrid grand canonical Monte Carlo simulation

The adsorption behavior of CO_2 in MOFs was calculated by hybrid grand canonical Monte Carlo (H-GCMC) simulations. In this simulation, the usual GCMC moves of translation, rotation, insertion and deletion trials were used for the adsorbate molecules. In addition, to describe the framework flexibilities of MOFs on gas adsorption, three additional moves were adopted, *i.e.*, framework atom translation, volume change as well as hybrid Monte Carlo (HMC). In the HMC move, the unit cell is isotropically scaled and kept orthorhombic. A small *NVE* MD simulation with Velocity-Verlet algorithm was employed. The initial velocities of the framework atoms and adsorbate molecules were randomly sampled from a Maxwell-Boltzmann distribution, and the system was integrated using time step 0.5 fs for 5 MD steps to obtain a new configuration. Details of the simulation method can be found in the work of Dubbeldam et al. [20]. The simulations were carried out for one unit cell at 298 K. A cutoff radius of 12 Å was applied to the LJ interactions, and the long-range electrostatic interactions were handled

using the Ewald summation technique. Periodic boundary conditions were applied in all three dimensions. The frequencies of all MC moves were 0.15 and their acceptation rates are listed in Table 2. For each state point, H-GCMC simulation consisted of 1×10^7 steps to guarantee equilibration followed by 2×10^7 steps to sample the desired thermodynamic properties. Test simulations using $2\times2\times2$ unit cells gave equivalent results, but were deemed too expensive for the computational cost. The output of such a simulation is the absolute amount adsorbed, while in experiments the excess amount adsorbed is measured. Thus, translation between absolute and excess amounts is required, and the method can be found in Ref. [4]

Results and discussion

Force field development

The atom types are shown in Fig. 1b. It should be noted that O(1) and O(2) are equivalent except in the O-Cu-O angle types. So we just use O instead of O(1) and O(2) in bond stretching, dihedral angle, improper torsion and other angle bending types. The potentials are described by Eqs. 1–5.

$$E_{nobond} = \frac{q_i q_j}{r} + 4\varepsilon_{ij}\left[\left(\frac{\sigma_{ij}}{r}\right)^{12} - \left(\frac{\sigma_{ij}}{r}\right)^6\right] \tag{1}$$

$$E_{bond} = D\left[1 - e^{-\alpha(b-b_0)}\right]^2 \tag{2}$$

$$E_{angle} = K_\theta(\theta - \theta_0)^2 \tag{3}$$

Table 2 GCMC statistics for CO_2 at 0.1 MPa and 298 K

Move	Acceptance (%)
Translation in x-direction	52.4058
Translation in y-direction	52.4300
Translation in z-direction	53.2221
Random rotation	50.0836
Regrow	2.6300
Insertion	12.3671
Deletion	12.3923
Volume	50.8589
Hybrid	90.4626

$$E_{torsions} = K_\varphi[1 + d\cos(n\varphi)] \qquad (4)$$

$$E_{imp.tor.} = K_\chi[1 + d\cos(n\chi)], \qquad (5)$$

where q is a charge parameter. ε and σ are the Lennard-Jones (LJ) potential parameters for the interactions between atoms i and j. b, θ, φ, χ and r are bond length, valence angle, torsion angle, improper torsion angle, and non-bonded distance, respectively. D, K_θ, K_φ and K_χ are the force constants for the corresponding interactions. b_0 and θ_0 are the equilibrium bond length and angle, n is the periodicity.

First, the non-bonded interaction parameters were selected. The partial charges were taken from our previous work [27], and the van der Waals parameters were extracted from Dreiding force field [12] (Cu from UFF [11]) directly; the advantage of using Dreiding force field to describe the interactions between adsorbates and MOFs is that this force field has been validated many times for its accuracy in describing the adsorption of gases in various MOFs. Thus, the new force field can retain the accuracy for gas adsorption in Cu-BTC. The mixed LJ parameters were obtained using the geometric mixing rule. Force field parameters for non-bonded interactions are listed in Table 3.

$$\varepsilon_{ij} = \sqrt{\varepsilon_{ii}\varepsilon_{jj}} \quad \text{and} \quad \sigma_{ij} = \sqrt{\sigma_{ii}\sigma_{jj}} \qquad (6)$$

For bonded interactions, they were divided into two parts: metal-oxide cluster and organic moiety. The metal-oxide cluster was described by a Cu-O bonded intramolecular term and O-Cu-O and Cu-O-C(1) angle intramolecular terms. At first, we have tried to use the DFT calculations to parameterize the harmonic potential for the Cu-O bonds, but the DFT calculations could not describe the Cu-O bonds well. So in our force field, we adopted Morse potential for all the bond stretching. The parameters (D and a) for Cu-O were taken from the tetra-coordinated copper(II) amino acidates force field developed by Kaitner et al. [31]. It should be pointed out that in the force field developed by Kaitner *et al.*, the given angle terms (such as O-Cu-N) are

Table 3 Force field parameters for non-bonded interactions

Atom type	q (e)	ε (kcal mol^{-1})	σ (Å)
Cu	1.098	0.005	3.114
O	−0.665	0.096	3.033
C(1)	0.778	0.095	3.473
C(2)	−0.092	0.095	3.473
C(3)	−0.014	0.095	3.473
H	0.109	0.015	2.846

describe by 1–3 interactions while harmonic model for others. This special treatment of the angle terms can make our force field difficult to use with the general MD codes. So, we used the harmonic model for all the angle bending, and only the O-Cu-O and Cu-O-C(1) angle bending parameters were obtained based on the DFT calculations. Vibrational frequency calculations validated that our optimized geometry for the model was a true minimum. We adopted a similar strategy suggested by Tafipolsky et al. [22] to parameterize our angle bending model. The Hessian matrix in Cartesian coordinates was obtained from optimization and frequency calculations and then it was transformed to a set of force constants in internal coordinates with the program SHRINK written by Sipachev [32]. At last only O-Cu-O and Cu-O-C(1) angle bending force constants were taken from the force constants in internal coordinates. The intramolecular force constants in organic moiety (D, a, K_θ, K_φ and K_χ) were extracted from the widely used CVFF force field [14].

In addition, two torsion terms Cu-O-C(1)-C(2) and Cu-O-C(1)-O were also included for interactions between the metal-oxide cluster and organic part, whose parameters (K_φ) were fitted by us to reproduce the NTE coefficient [16] with MD simulations. It should be pointed out that except the force constants and non-bonded parameters mentioned above, the equilibrium bond distances and angles (b_0 and θ_0) should also be input in the MD simulations, so they were taken from the experimental ones [25]. To examine the influence of the two torsion terms on the NTE property, calculations were performed with one parameter fixed while the other one changed. The results show that both of them have an effect on the flexibility and the influence is almost the same. So the two parameters were treated to be identical in our fitting procedure. With all the other force constants, non-bonded parameters and equilibrium values fixed, the force constants of the two torsion terms were adjusted until the NTE coefficient could be reproduced.

After fixing the force constants of the two torsion terms, some of the equilibrium bond distances (Cu-O, O-C(1), C(1)-C(2), C(2)-C(3)) and angles (O(1)-Cu-O(1), O(2)-Cu-O(2), O(1)-Cu-O(2), Cu-O-C(1), O-C(1)-O, O-C(1)-C(2)) taken from experimental values were modified slightly to make the simulated bond and angle values better agree with the corresponding experimental values, as well as the lattice parameters. Because the equilibrium bond distances and angles are required to calculate the NTE coefficient, the refined values were used to calculate the NTE coefficient again to check the sensitivity. The difference between the two results is within 3%, so the change is acceptable. Force field parameters for bonded interactions are listed in Table 4, in which the original values are given in parentheses for the refined ones to show the extent of adjustment. In addition,

Table 4 Force field parameters for bonded interactions

Bond type	D (kcal mol^{-1})	α (Å^{-1})	b_0 (Å)
Cu-O	85.769	2.85	1.969(1.952)
O-C(1)	135.00	2.00	1.260(1.252)
C(1)-C(2)	87.84	2.00	1.456(1.500)
C(2)-C(3)	120.0	2.00	1.355(1.397)
C(3)-H	116.0	1.77	0.931
Angle type	K_θ (kcal mol^{-1} rad^{-2})		θ_0 (degree)
O(1)-Cu-O(1)	50.160		170.2(168.2)
O(2)-Cu-O(2)	50.160		170.2(168.2)
O(1)-Cu-O(2)	12.000		90.0(89.1)
Cu-O-C(1)	40.470		127.5(123.0)
O-C(1)-O	145.000		128.5(125.6)
O-C(1)-C(2)	54.495		116.2(117.2)
C(1)-C(2)-C(3)	34.680		119.9
C(3)-C(2)-C(3)	90.000		120.1
C(2)-C(3)-C(2)	90.000		119.9
C(2)-C(3)-H	37.000		120.0
Dihedral type	K_φ (kcal mol^{-1})	d	n
Cu-O-C(1)-C(2)	3.00	−1	2
Cu-O-C(1)-O	3.00	−1	2
C(2)-C(3)-C(2)-C(3)	3.00	−1	2
C(1)-C(2)-C(3)-C(2)	3.00	−1	2
C(1)-C(2)-C(3)-H	3.00	−1	2
C(3)-C(2)-C(3)-H	3.00	−1	2
O-C(1)-C(2)-C(3)	2.50	−1	2
Improper torsion type	K_χ (kcal mol^{-1})	d	n
H-C(3)-C(2)-C(2)	0.37	−1	2
C(1)-C(2)-C(3)-C(3)	10.0	−1	2
C(2)-C(1)-O-O	10.0	−1	2

to calculate the adsorption isotherms of CO_2 in Cu-BTC, the EPM2 model [33] was used for CO_2/CO_2 and CO_2/ material interactions.

Comparison with experimental material properties

The lattice parameter of Cu-BTC at 293 K from the new force field is 26.324±0.005 Å, which is in good agreement with the experimental value of 26.328 Å [16]. The averaged bond and angle values also agree well with the experimental ones (Tables 5 and 6) [25]. The force field could

reproduce the bond distances within ±0.015 Å and angles within ±3°.

The simulated change in the lattice parameter of Cu-BTC with temperature is shown in Fig. 2. Experimentally, Wu et al. obtained an average linear coefficient of thermal expansion $\alpha = (1/L_0)(dL/dT) = -4.1 \times 10^{-6} K^{-1}$ from

Table 5 Averaged bond lengths (Å) for Cu-BTC at 293 K

Bond	Simulated	Experimental [25]
Cu-O	1.947	1.952
O-C(1)	1.240	1.252
C(1)-C(2)	1.500	1.500
C(2)-C(3)	1.395	1.397
C(3)-H	0.941	0.931

Table 6 Averaged angles (degree) for Cu-BTC at 293 K

Angle	Simulated	Experimental [25]
O(1)-Cu-O(1)	168.5	168.2
O(2)-Cu-O(2)	168.5	168.2
O(1)-Cu-O(2)	86.1	89.1
Cu-O-C(1)	124.1	123.0
O-C(1)-O	126.2	125.6
O-C(1)-C(2)	116.6	117.2
C(1)-C(2)-C(3)	121.3	119.9
C(2)-C(3)-C(2)	121.3	119.9
C(3)-C(2)-C(3)	118.4	120.1
C(2)-C(3)-H	119.1	120.0

Fig. 2 Temperature dependency of the simulated lattice parameters of Cu-BTC calculated from MD simulations. Error bars indicate uncertainties in the simulated lattice parameters

Fig. 3 Energy-volume graphs used to obtain the bulk modulus (B_0) from MD simulation at 300 K

80 to 500 K [16], which agrees quite well with the value of $-4.7 \times 10^{-6} K^{-1}$ obtained in our simulations in this range from Fig. 2, demonstrating that the new force field reproduces well this unusual NTE behavior of Cu-BTC.
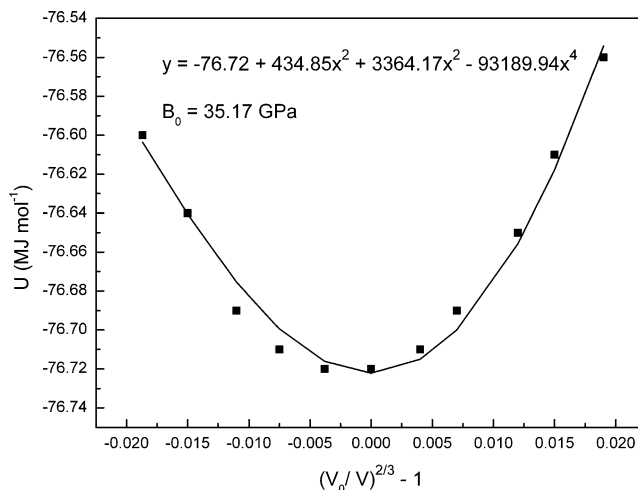
We further examined the vibrational motion of Cu-BTC at 298 K. The experimental low-frequency Raman modes observed on the Cu-BTC reported by Prestipino et al. [34] provide a basis for comparison. In their work, Prestipino et al. [34] pointed out that the frequency of 228 cm^{-1} is for Cu-Cu stretching and our DFT calculated frequency for the same mode is 240 cm^{-1}; the two values are quite close. Furthermore, the power spectrum for Cu was computed with MD simulations using the new force field, and the corresponding frequency is 234 cm^{-1}, quite close to the experimental value of 228 cm^{-1} [34]. It should be pointed out that the force field parameters were not refined to match the vibrational frequency, thus, the calculated result with the new force field is a predictive one.
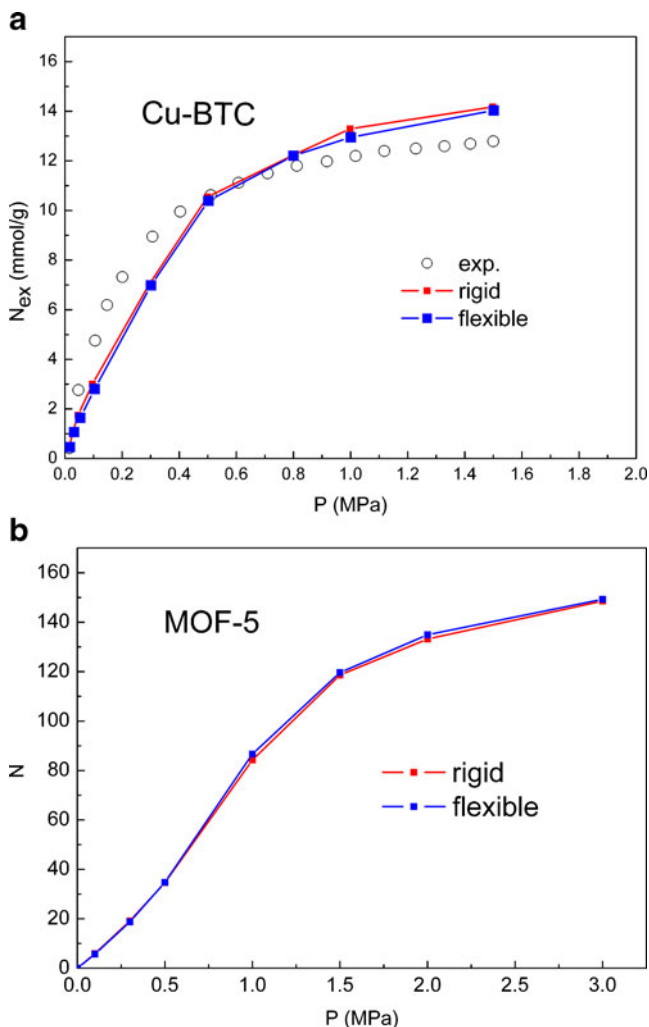
Prediction of mechanical properties

As a first step to study the dynamic behavior of Cu-BTC and compared with another well-studied MOF, MOF-5, we calculated the bulk modulus (B_0) using the new force field by fitting energy-volume results to the equations of state as follows [35]

$$U = U_0 + \frac{9}{8}B_0 V_0 \left[\left(\frac{V_0}{V}\right)^{2/3} - 1\right]^2$$
$$+ \frac{9}{16}B_0 V_0 (B_p - 4)\left[\left(\frac{V_0}{V}\right)^{2/3} - 1\right]^3 \quad (7)$$
$$+ \gamma_4 \left[\left(\frac{V_0}{V}\right)^{2/3} - 1\right]^4 + \cdots,$$

where U is the potential energy, V_0 and V are the equilibrium volume and strained volume, respectively. B_0 is bulk modulus and B_p is the derivative of the bulk

Fig. 4 Comparison of rigid and flexible frameworks of CO_2 adsorption in (a) Cu-BTC and (b) MOF-5 at 298 K

modulus with pressure. For the studied crystals the first four terms are enough to obtain a good fit. Figure 3 shows that the predicted bulk modulus (B_0) of Cu-BTC at 300 K is 35.17 GPa using the new force field, which is much higher than the simulated result of MOF-5 (4.0 GPa) obtained by Greathouse and Allendorf [19]. The results show that it is more difficult to compress Cu-BTC than MOF-5 under pressuring. On the other hand, Cu-BTC also shows a smaller NTE coefficient than MOF-5, indicating it also contracts less than MOF-5 under heating. The two properties together clearly demonstrate that Cu-BTC is less flexible than MOF-5.

Prediction of the influences of dynamics of Cu-BTC framework on CO_2 adsorption

The adsorption isotherms of CO_2 in rigid and flexible Cu-BTC frameworks at 298 K were further calculated, and the results are shown in Fig. 4. Obviously, the new force field reproduces well the experimental results of CO_2 adsorption [36]. On the other hand, Fig. 4 shows that the effect of framework flexibility is insignificant for CO_2 adsorption in Cu-BTC at 298 K. To make a comparison with MOF-5, parallel simulations were also performed for MOF-5 with the flexible force field developed by Dubbeldam et al. [20]. Figure 4 shows that a similar trend was observed for CO_2 adsorption in MOF-5. The similar result was recently demonstrated by Greathouse et at. [37].

It is widely recognized that the flexibility of MOFs has a more pronounced effects on gas diffusivity as well as the systems with strong adsorbate/MOF interactions. For example, the work of Amirjalayer et al. [23] demonstrates that framework flexibility can lead to a change in order of magnitude for benzene self-diffusion coefficient in MOF-5. So, we believe the new force field is more useful for studying diffusion and the systems with strong adsorbate/Cu-BTC interactions.

Conclusions

In this work, we reported a new force field for describing the flexibility of Cu-BTC. The comparisons with experimental structural parameters, NTE behavior, vibrational frequency of Cu-BTC, as well as CO_2 adsorption isotherm show that the new force field is reliable. Also the present work demonstrates that Cu-BTC is much less flexible than MOF-5. One point which should be emphasized is that since Dreiding force field was adopted to describe the adsorbate/MOF interactions, the new force field remains the reliability of Dreiding force field for describing gas adsorption in MOFs. The approach can be readily extended to other MOFs. Currently, we are doing investigations on

the understanding of the dynamic behavior of the pockets in Cu-BTC using the new force field.

References

1. Férey G (2008) Hybrid porous solids: past, present, future. Chem Soc Rev 37:191–214. doi:10.1039/b618320b
2. Snurr RQ, Hupp JT, Nguyen ST (2004) Prospects for nanoporous metal-organic materials in advanced separations processes. AIChE J 50:1090–1095. doi:10.1002/aic.10101
3. Rowsell JLC, Yaghi OM (2005) Strategies for hydrogen storage in metal-organic frameworks. Angew Chem Int Ed 44:4670–4679. doi::10.1002/anie.200462786
4. Düren T, Sarkisov L, Yaghi OM, Snurr RQ (2004) Design of new materials for methane storage. Langmuir 20:2683–2689. doi:10.1021/la0355500
5. Yang Q, Zhong C (2005) Molecular simulation of adsorption and diffusion of hydrogen in metal-organic frameworks. J Phys Chem B 109:11862–11864. doi:10.1021/jp051903n
6. Garberoglio G, Skoulidas AI, Johnson JK (2005) Adsorption of gases in metal organic materials: comparison of simulations and experiments. J Phys Chem B 109:13094–13103. doi:10.1021/jp050948l
7. Skoulidas AI, Sholl DS (2005) Self-diffusion and transport diffusion of light gases in metal-organic framework materials assessed using molecular dynamics simulations. J Phys Chem B 109:15760–15768. doi:10.1021/jp051771y
8. Yang Q, Zhong C (2006) Electrostatic-field-induced enhancement of gas mixture separation in metal-organic frameworks: a computational study. ChemPhysChem 7:1417–1421. doi:10.1002/cphc.200600191
9. Düren T, Snurr RQ (2004) Assessment of isoreticular metal-organic frameworks for adsorption separations: a molecular simulation study of methane/*n*-butane mixtures. J Phys Chem B 108:15703–15708. doi:10.1021/jp0477856
10. Ramsahye NA, Maurin G, Bourrelly S, Llewellyn P, Loiseau T, Férey G (2007) Charge distribution in metal organic framework materials: transferability to a preliminary molecular simulation study of the CO_2 adsorption in the MIL-53 (Al) system. Phys Chem Chem Phys 9:1059–1063. doi:10.1039/b613378a
11. Rappé AK, Casewit CJ, Colwell KS, Goddard WA, Skiff WM (1992) UFF, a full periodic table force field for molecular mechanics and molecular dynamics simulations. J Am Chem Soc 114:10024–10035. doi:10.1021/ja00051a040
12. Mayo SL, Olafson BD, Goddard WA (1990) DREIDING: a generic force field for molecular simulations. J Phys Chem 94:8897–8909. doi:10.1021/j100389a010
13. Jorgensen WL, Maxwell DS, Tirado-Rives J (1996) Development and testing of the OPLS all-atom force field on conformational energetics and properties of organic liquids. J Am Chem Soc 118:11225–11236. doi:10.1021/ja9621760
14. Dauber-Osguthorpe P, Roberts VA, Osguthorpe DJ, Wolff J, Genest M, Hagler AT (1988) Structure and energetics of ligand binding to proteins: *Escherichia coZi* dihydrofolate reductase-trimethoprim, a drug-receptor system. Proteins: Struct, Function, Bioinformat 4:31–47. doi:10.1002/prot.340040106
15. Bourrelly S, Llewellyn PL, Serre C, Millange F, Loiseau T, Férey G (2005) Different adsorption behaviors of methane and carbon

dioxide in the isotypic nanoporous metal terephthalates MIL-53 and MIL-47. J Am Chem Soc 127:13519–13521. doi:10.1021/ja054668v

16. Wu Y, Kobayashi A, Halder GJ, Peterson VK, Chapman KW, LockN SPD, Kepert CJ (2008) Negative thermal expansion in the metal-organic framework material Cu3(1, 3, 5-benzenetricarboxylate)2. Angew Chem Int Ed 47:8929–8933. doi:10.1002/anie.200803925

17. Uemura K, Matsuda R, Kitagawa S (2005) Flexible microporous coordination polymers. J Solid State Chem 178:2420–2429. doi:10.1016/j.jssc.2005.05.036

18. Greathouse JA, Allendorf MD (2006) The interaction of water with MOF-5 simulated by molecular dynamics. J Am Chem Soc 128:10678–10679. doi:10.1021/ja063506b

19. Greathouse JA, Allendorf MD (2008) Force field validation for molecular dynamics simulations of IRMOF-1 and other isoreticular zinc carboxylate coordination polymers. J Phys Chem C 112:5795–58002. doi:10.1021/jp076853w

20. Dubbeldam D, Walton KS, Ellis DE, Snurr RQ (2007) Exceptional negative thermal expansion in isoreticular metal-organic frameworks. Angew Chem Int Ed 46:4496–4499. doi:10.1002/anie.200700218

21. Huang BL, McGaughey AJH, Kaviany M (2007) Thermal conductivity of metal-organic framework 5 (MOF-5): part I. Molecular dynamics simulations. Int J Heat Mass Transfer 50:393–404. doi:10.1016/j.ijheatmasstransfer.2006.10.002

22. Tafipolsky M, Amirjalayer S, Schmid R (2007) Ab initio parametrized MM3 force field for the metal-organic framework MOF-5. J Comput Chem 28:1169–1176. doi:10.1002/jcc.20648

23. Amirjalayer S, Tafipolsky M, Schmid R (2007) Molecular dynamics simulation of benzene diffusion in MOF-5: importance of lattice dynamics. Angew Chem Int Ed 46:463–466. doi:10.1002/anie.200601746

24. Salles F, Ghoufi A, Maurin G, Bell RG, Mellot-Draznieks C, Férey G (2008) Molecular dynamics simulations of breathing MOFs: structural transformations of MIL-53(Cr) upon thermal activation and CO2 adsorption. Angew Chem Int Ed 47:8487–8491. doi:10.1002/anie.200803067

25. Chui SS-Y, Lo SM-F, Charmant JPH, Orpen AG, Williams ID (1999) A chemically functionalizable nanoporous material [Cu3(TMA)2(H2O)3]n. Science 283:1148–1150. doi:10.1126/science.283.5405.1148

26. Vishnyakov A, Ravikovitch PI, Neimark AV, Bülow M, Wang QM (2003) Nanopore structure and sorption properties of Cu-BTC metal-organic framework. Nano Lett 3:713–718. doi:10.1021/nl0341281

27. Yang Q, Zhong C (2006) Molecular simulation of carbon dioxide/methane/hydrogen mixture adsorption in metal-organic frameworks. J Phys Chem B 110:17776–17783. doi:10.1021/jp062723w

28. Frisch MJ, Truchks GW, Schlegel HB et al (2003) Gaussian 03 Rev B1. Gaussian Inc, Pittsburgh

29. Plimpton SJ, Pollock R, Stevens M (1997) Particle-Mesh Ewald and rRESPA for parallel molecular dynamics simulations. Eighth SIAM Conference on Parallel Processing for Scientific Computing

30. Plimpton SJ (1995) Fast parallel algorithms for short-range molecular dynamics. J Comput Phys 117:1–19

31. Kaitner B, Paulić N, Pavlović G, Sabolović J (1999) Bis(L-N, N-dipropylalaninato)copper(II) X-ray crystal structure, the crystal structure prediction and conformational analysis with a new force field. Polyhedron 18:2301–2311. doi:10.1016/S0277-5387(99)00128-X

32. Sipachev VA (1985) Calulation of shrinkage corrections in harmonic approximation. J Mol Struct, Theochem 121:143–151

33. Harris JG, Yung KH (1995) Carbon dioxide's liquid-vapor coexistence curve and critical properties as predicted by a simple molecular model. J Phys Chem 99:12021–12024

34. Prestipino C, Regli L, Vitillo JG, Bonino F, Damin A, Lamberti C, Zecchina A, Solari PL, Kongshaug KO, Bordiga S (2006) Local structure of framework Cu(II) in HKUST-1 metallorganic framework: spectroscopic characterization upon activation and interaction with adsorbates. Chem Mater 18:1337–1346. doi:10.1021/cm052191g

35. Valencia F, Romero AH, Hernandez E, Terrones M, Terrones H (2003) Theoretical characterization of several models of nanoporous carbon. New J Phys 5:123.1–123.16

36. Liang Z, Marshall M, Chaffee AL (2009) CO2 adsorption-based separation by metal organic framework (Cu-BTC) versus zeolite (13X). Energy Fuels 23:2785–2789. doi:10.1021/ef800938e

37. Greathouse JA, Kinnibrugh TL, Allendorf MD (2009) Adsorption and separation of noble gases by IRMOF-1: grand canonical Monte Carlo simulations. Ind Eng Chem Res 48:3425–3431. doi:10.1021/ie801294n